Optimized transition-edge x-ray microcalorimeter with 2.4 eV energy resolution at 5.9 keV

J. N. Ullom,[a] J. A. Beall, W. B. Doriese, W. D. Duncan, L. Ferreira, G. C. Hilton,
K. D. Irwin, C. D. Reintsema, and L. R. Vale
National Institute of Standards and Technology (NIST), 325 Broadway, Boulder, Colorado 80305

We present measurements from a series of transition-edge x-ray microcalorimeters designed for optimal energy resolution. We used the geometry of the sensors to control their heat capacity and employed additional normal metal features and a perpendicular magnetic field to control the sharpness of the superconducting-to-normal transition. These degrees of control allow an optimal selection of sensor saturation energy and noise. Successive design changes improved the measured energy resolution of the sensors from 4.5 eV full width at half maximum at 5.9 keV to 2.4 eV at 5.9 keV. Sensors with this energy resolution are well matched to applications in x-ray astrophysics and terrestrial materials analysis.
[DOI: 10.1063/1.2061865]

Transition-edge sensors (TESs) are a promising technology for high-resolution x-ray spectroscopy.[1] These sensors consist of superconducting thin films electrically biased in the resistive transition. The ability of TESs to perform broadband, high-efficiency, and high-resolution x-ray spectroscopy makes them powerful tools for x-ray astronomy and terrestrial materials analysis.[2,3] The best energy resolutions obtained so far with TESs [approximately 4 eV full width at half maximum (FWHM) at 5.9 keV] are roughly 30 times better than ubiquitous silicon-lithium sensors.[4–6] Despite this impressive performance, the resolution of TESs has not yet reached the predicted theoretical limits and has shown little improvement in recent years. Given the large range of applications, there is considerable interest in improving sensor performance. For instance, an energy resolution of 2 eV FWHM at 5.9 keV is the goal for the upcoming National Aeronautic and Space Administration (NASA) satellite Constellation-X.[7]

The commonly assumed sources of noise in TESs are Johnson noise and thermodynamic fluctuations in the device thermal conductances. One factor that limits sensor performance is the presence of noise that is not explained by these two mechanisms. In recent work, we characterized the dependencies of the unexplained noise (UN) and predicted how the design of TES sensors could be optimized.[8] The most promising optimization strategy was to make sensors with low heat capacity, a broad superconducting-to-normal transition, and low UN. In this letter, we present results from three optimized TES x-ray microcalorimeters. All three sensors perform better than those in previous work, and the best device has an energy resolution of 2.4±0.1 eV FWHM at 5.9 keV. We also discuss possible future performance levels.

The energy resolution of a TES microcalorimeter depends on its transition temperature T_c, heat capacity C, the UN, and the sharpness of the superconducting-to-normal transition, described by the dimensionless parameter $\alpha = (T/R)dR/dT$, where R is the sensor resistance. For simplicity, we take $\beta_I = (I/R)\partial R/\partial I$ to be zero, although this quantity is known to be finite. We have modified the traditional expression for the resolution of a TES (Ref. 9) to include finite bath temperatures, finite loop gain, and degradation by the UN. The UN is treated as a white voltage noise whose magnitude M is expressed as a fraction of the zero-inductance high-frequency limit of the Johnson noise. Assuming a stiff voltage bias, the FWHM energy resolution ΔE_{FWHM} is given by

$$2.355 \sqrt{\frac{4k_b T_c^2 C n(1+M^2)}{\alpha^2(1-t^n)}} \sqrt{1 + \frac{\alpha^2(1-t^n)F}{n(1+M^2)}}, \qquad (1)$$

where n is the exponent governing power flow between the TES and the heat bath (typically 3–5), $t=T_b/T_c$ is the ratio of the bath and transition temperatures, and F depends on the nature of energy transport between the TES and the bath. For specular transport, $F=(1+t^{n+1})/2$, and for diffuse, $F=n(1-t^{2n+1})/((2n+1)(1-t^n))$.[10,11] In the limits $T_b \ll T_c$ and $\alpha^2/(1+M^2) \gg 2n$, Eq. (1) approximates to $\Delta E_{\text{FWHM}}=2.355\sqrt{(4k_b T_c^2 C/\alpha)\sqrt{(1+M^2)n/2}}$. It can readily be seen that sensor performance is improved by lowering T_c and C. The narrow temperature range over which the TES resistance responds to temperature imposes an additional constraint on C and α: namely, the device must retain temperature sensitivity during the temperature excursion $\Delta T=E_\gamma/C$ produced by the absorption of a photon with energy E_γ. The maximum photon energy $E_{\gamma\text{-max}}$ that a sensor can measure without performance degradation from nonlinearity will be proportional to C/α since α is inversely proportional to the temperature width of the transition.

We next describe two strategies for optimizing the energy resolution of a TES microcalorimeter. These strategies build on the results of Ref. 8, in which we found that the magnitude of the UN increases with α. For the conditions in Ref. 8, $M \sim 0.2\alpha^{1/2}$. In addition, we found that α could be controllably suppressed from intrinsic values greater than 500 to as low as 10 by the application of a perpendicular magnetic field or by incorporating normal-metal regions into the TES perpendicular the direction of current flow. We consider first the case where the TES heat capacity is fixed. This constraint arises if other system requirements dictate the pixel size. Substituting the expression for M into Eq. (1), we

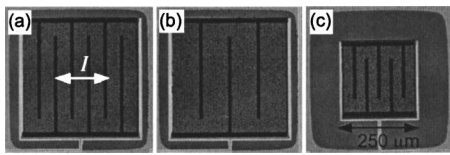[a]Electronic mail: ullom@boulder.nist.gov

FIG. 1. (a)–(c) Photographs of TES x-ray microcalorimeters A–C. The normal Cu bars are visible underneath the Bi absorbers and appear dark. The superconducting Mo leads appear light. The white arrow indicates the direction of the bias Current I in all devices. The scale is identical in the three photographs.

find that sensor performance is maximized by maximizing α, even though the UN is increased. Hence, when C is fixed, α should be increased until $E_{\gamma\text{-max}}$ is matched to the peak photon energy of interest. We consider second the case where C can be treated as a free parameter. Here, it is desirable to simultaneously reduce C and α while keeping the ratio C/α constant so that $E_{\gamma\text{-max}}$ is matched to the peak photon energy of interest. The low value of α reduces the UN and improves the energy resolution.

To demonstrate these optimization strategies, we fabricated three TES x-ray microcalorimeters with transition temperatures near 115 mK. The devices consisted of bilayers of Mo and Cu with a 1.5 μm overlayer of Bi to increase the x-ray stopping power. The devices include an additional Cu layer for edge passivation and the normal metal features that suppress α. The devices were suspended on 0.4 μm thick Si_3N_4 membranes. Photographs are shown in Fig. 1. The low normal-state resistance of the devices, ~ 11 mΩ, minimizes their internal thermal impedance. The devices were operated in an adiabatic demagnetization refrigerator at bath temperatures of 60–70 mK. A small superconducting coil was used to control the magnetic field perpendicular to the plane of the devices, and 5.9 keV x-rays were supplied by a ^{55}Fe source. The devices were operated with a stiff voltage bias and the signal currents were measured with a two-stage superconducting quantum interference device ammeter.

Device designs fall on the C-α plane, shown in Fig. 2. Dashed lines through the origin correspond to a constant $E_{\gamma\text{-max}}$. Methods used to determine C, α, and $E_{\gamma\text{-max}}$ will be given later. First, however, we describe the key differences between Devices A–C. Device A was 400 μm on a side and had six perpendicular normal bars to reduce α and M. Previous devices with these dimensions but without the bars had an energy resolution of 4.5 eV.[4] The best resolution obtained with Device A was 3.2 eV when the perpendicular field was zero and α was the highest. However, even in zero field,
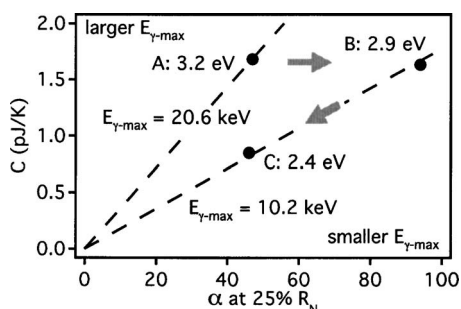

FIG. 2. Parameter space for transition-edge sensor design. Sensor heat capacity is plotted on the vertical axis. Transition steepness $\alpha = (T/R) \times (dR/dT)$ at $R/R_N = 0.25$ is plotted on the horizontal axis. Dashed lines are lines of constant $E_{\gamma\text{-max}}$. The positions and performance of Sensors A–C are shown in the plot. Best sensor performance is achieved close to the origin of the plot with $E_{\gamma\text{-max}}$ well matched to the peak photon energy of interest.
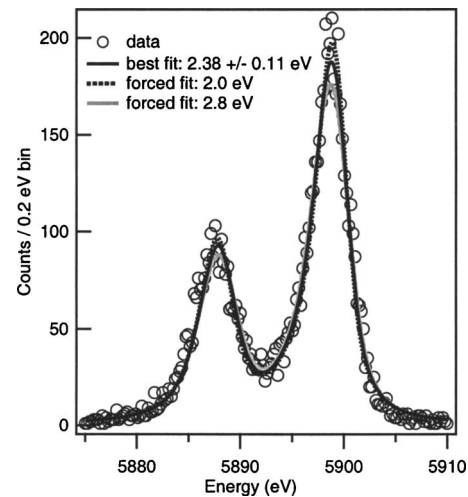

FIG. 3. Pulse height spectrum of the Mn $K\alpha$ complex measured with Device C. The displayed region of the histogram contains 7754 counts obtained over 3700 s. Pulse heights were obtained by applying a conventional colored-noise optimal filter to digitized pulse records. The solid curve is the result of least-squares fitting to the spectral database of Holzer as modified by Porter (Refs. 12 and 13). The instrumental energy resolution predicted from the fitting is 2.38±0.11 eV FWHM. For comparison, the dashed and gray curves show least-squares fits where the instrumental resolution was fixed at 2.0 and 2.8 eV, respectively.

Device A was far from saturation; Device A lies on the line for $E_{\gamma\text{-max}} = 20.6$ keV. To test optimization Strategy 1, we fabricated Device B with only three normal bars to increase α and better match $E_{\gamma\text{-max}}$ to 5.9 keV. Since the bars make only a small contribution to C, this change corresponds to horizontal motion to the right in Fig. 2. $E_{\gamma\text{-max}}$ of Device B was close to 10.2 keV and the energy resolution improved to 2.9 eV. To test optimization Strategy 2, we fabricated Device C, which was 250 μm on a side and had five normal metal bars. Because of its smaller size, the heat capacity of Device C was roughly one-half of the heat capacity of Device B (and A). The change from three to five bars reduced α by a similar factor, thus maintaining $E_{\gamma\text{-max}}$ near 10.2 keV. Hence, the change from B to C corresponds to motion toward the origin of Fig. 2 along the line corresponding to $E_{\gamma\text{-max}} = 10.2$ keV. For both Devices B and C, best results were achieved using a small magnetic field to broaden the transition. Device C had the lowest α, the lowest M, and the best resolution of the three devices. As shown in Fig. 3, the resolution of Device C was 2.4 eV at 5.9 keV. This result is the best resolution obtained with any energy-dispersive measurement technology.

Additional insight can be obtained from the device parameters in Table I. The first group (T_c, R_N, G_o, and C) is largely independent of bias point. The differential thermal conductance $G_o = dP/dT$ was obtained from current-voltage curves at a range of bath temperatures. Heat capacity was obtained from the resistance change induced by 5.9 keV x-rays and curves of resistance versus internal temperature generated as in Ref. 14.

The second group of parameters describes the experimentally determined optimal bias point. The operating resistance R, bias power P_b, and bias current I were all obtained from measured current-voltage curves. The transition steepness in the small signal limit α_{SSL} was obtained in two ways: First, from the slope of resistance versus temperature curves obtained under bias, and second, from fitting digitized x-ray pulses with a single exponential time constant τ_{20-0} as they decay from 20% of their peak value back to the baseline

TABLE I. Device parameter summary.

Parameter	Device A	Device B	Device C
T_c	115 mK	118 mK	110 mK
R_N	11.5 mΩ	12.8 mΩ	10.5 mΩ
G_o	670 pW/K	718 pW/K	323 pW/K
C	1.68 pJ/K	1.63 pJ/K	0.85 pJ/K
R	5.54 mΩ	3.27 mΩ	1.76 mΩ
P_b	20.3 pW	21.8 pW	9.0 pW
I	60.5 μA	81.6 μA	71.4 μA
Magnetic field	0 G	1.4 mG	5.0 mG
α_{SSL}	80–83	94–217	59–114
M	1.0	1.5–1.8	1.2–1.4
$E_{\gamma\text{-max}}$	20.6 keV	10.2 keV	10.2 keV
PH	17.2 μA	41.0 μA	32.8 μA
$R_{\max}$	7.77 mΩ	6.75 mΩ	3.42 mΩ
α_{LSL}	59	104	41
τ	152 μs	82 μs	261 μs
ΔE_{FWHM} pred.	3.0 eV	2.9 eV	2.7 eV
ΔE_{FWHM} meas.	3.2±0.1 eV	2.9±0.1 eV	2.4±0.1 eV

$[\alpha_{\mathrm{SSL}}=(G_oT_c/P_b)(C/(G_o\tau_{20\text{-}0})-1)]$. This second method was used to obtain the values of α given in Fig. 2. The two methods differed by up to a factor of 2, with the decay-time method consistently providing lower values. As a result, a range for α_{SSL} is given in Table I. The lower values obtained from the decay times are likely more accurate, since the computed resistance-temperature curves become unphysically sharp in devices with high α, such as Device B. The excess noise M was computed from measurements of the current spectral density as in Ref. 8. A range for M is given because of the uncertainty in α_{SSL}. The values for M in Table I are not expected to scale as $\alpha^{1/2}$, since the three devices were biased at different resistance fractions. A notable consequence of the normal bars in Device C is that even as low in the transition as $R/R_N=0.17$, $M=1$. At a similar resistance fraction, a device with no bars (and in 10 mG) had $M=8.7$.[8] Hence, bars allow TESs to be operated significantly lower in the transition.

To compute a peak photon energy $E_{\gamma\text{-max}}$ for Table I, we start with the relation $E_{\gamma\text{-max}}=fC\Delta T_w$, where ΔT_w is the temperature width of the transition and f is the maximum fractional temperature excursion. We assume a linear model for the transition shape so that $\alpha_{\mathrm{SSL}}=(T_c/R)(R_N/\Delta T_w)$. We further assume a bias fraction $R/R_N=0.25$ (a compromise between Devices A–C) and $f=0.2$ since an excursion of this magnitude halves the expected separation between the Mn $K\beta$ and Mn $K\alpha$ peaks, evidence of significant nonlinearity. Consequently, $E_{\gamma\text{-max}}=0.8CT_c/\alpha_{\mathrm{SSL}}$, where α_{SSL} is evaluated at $R/R_N=0.25$. This expression is only an approximation however, it provides a good measure for comparing devices.

The third group of parameters in Table I is relevant to Mn $K\alpha$ x rays. The measured current amplitude of the x-ray pulses is given by PH. The device resistance at the peak of the pulse is $R_{\max}$.[15] The parameter α is given in the large-signal limit (LSL) (α_{LSL}), where the LSL is the average over the excursion produced by a 5.9 keV(=0.94 fJ) Mn $K\alpha$ x ray. The LSL value of α was obtained in two ways: First, from the height of the x-ray pulses $[\alpha_{\mathrm{LSL}}=PH\,C\,T_c/(I\,0.94\,\mathrm{fJ})]$,

and second, from fitting pulses to a single exponential as they decay from 90% to 10% of their peak value. The two methods agreed so closely that only a single value for α_{LSL} is given. The time constants obtained from the 90–10 fitting are given in Table I as τ.

Predictions for the energy resolution were generated using Eq. (1), C, α_{LSL}, and M. Unlike α_{SSL}, α_{LSL} correctly accounts for the transition shape and hence the signal size. Additionally, the Johnson and phonon noise during a pulse are best captured by α_{LSL}. We used M measured at the bias point for convenience; an average over the pulse is more accurate but difficult to measure. Nonetheless, Table I shows excellent agreement between the measured and predicted values of ΔE. It can also be seen that the device parameters in Table I closely correspond to the picture of device optimization diagrammed in Fig. 2.

Further performance improvements will be possible with small changes to device parameters. For instance, we have previously demonstrated that M can be reduced to as low as 0.5 in low α devices.[8] If we lower α to achieve $M=0.5$ while holding $E_{\gamma\text{-max}}$ fixed, the resolution predicted from scaling the performance of Device C is 2.0 eV. In the future we will apply the optimization strategies described here to design sensors optimized for other energies. For photon energy E_γ, the resolution predicted by scaling the result of Device C is 2.4 eV$\sqrt{E_\gamma/5.9\text{ keV}}$. A device optimized for measuring chemical shifts in x-ray lines below 1.5 keV is predicted to have a resolution of 1.2 eV.

[1] K. D. Irwin, G. C. Hilton, D. A. Wollman, and J. M. Martinis, Appl. Phys. Lett. **69**, 1945 (1996).
[2] F. Scott Porter, Nucl. Instrum. Methods Phys. Res. A **520**, 354 (2004).
[3] D. A. Wollman, K. D. Irwin, G. C. Hilton, L. L. Dulcie, D. E. Newbury, and J. M. Martinis, J. Microsc. **188**, 196 (1997).
[4] K. D. Irwin, G. C. Hilton, J. M. Martinis, S. Deiker, N. Bergren, S. W. Nam, D. A. Rudman, and D. A. Wollman, Nucl. Instrum. Methods Phys. Res. A **444**, 184 (2000).
[5] W. M. Bergmann Tiest, H. F. C. Hoevers, M. P. Bruijn, W. A. Mels, M. L. Ridder, P. A. J. de Korte, and M. E. Huber, AIP Conf. Proc. **605**, 199 (2002).
[6] C. K. Stahle, R. P. Brekosky, E. Figueroa-Feliciano, F. M. Finkbeiner, J. D. Gygax, M. J. Li, M. A. Lindeman, F. Scott Porter, and N. Tralshawala, Proc. SPIE **4140**, 367 (2000).
[7] See ⟨http://constellation.gsfc.nasa.gov/science/example_science/endpoints.html⟩
[8] J. N. Ullom, W. B. Doriese, G. C. Hilton, J. A. Beall, S. Deiker, W. D. Duncan, L. Ferreira, K. D. Irwin, C. D. Reintsema, and L. R. Vale, Appl. Phys. Lett. **84**, 4206 (2004).
[9] K. D. Irwin, Appl. Phys. Lett. **66**, 1998 (1995).
[10] W. S. Boyle and K. F. Rodgers, J. Opt. Soc. Am. **49**, 66 (1959).
[11] S. H. Moseley, J. C. Mather, and D. McCammon, J. Appl. Phys. **56**, 1257 (1984).
[12] G. Holzer, M. Fritsch, M. Deutsch, J. Hartwig, and E. Forster, Phys. Rev. A **56**, 4554 (1997).
[13] F. Scott Porter (personal communication).
[14] D. T. Chow, A. Loshak, M. L. van den Berg, M. Frank, T. W. Barbee, Jr., and S. E. Labov, Proc. SPIE **4141**, 67 (2000).
[15] The fractional resistance changes from Mn $K\alpha$ x rays range from 16% to 27% of R_N and the observed ratios of the Mn $K\beta$ and Mn $K\alpha$ peak heights were greater than 1.07, whereas the natural ratio is 1.10. In contrast, the ratio predicted by the linear transition model for $R/R_N=0.25$ and $f=0.2$ is 1.05. Hence, the devices are more linear than predicted by the simple linear transition model.